

CROSS-POLAR AIRCRAFT TRAJECTORY OPTIMIZATION AND THE POTENTIAL CLIMATE IMPACT

Hok K. Ng, University of California, Santa Cruz, Moffett Field, CA 94035

Banavar Sridhar, Shon Grabbe, Neil Chen, NASA Ames Research Center, Moffett Field, CA 94035

Abstract

Cross-Polar routes offer new opportunities for air travel markets. Transpolar flights reduce travel times, fuel burns, and associated environmental emissions by flying direct paths between many North American and Asian cities. This study evaluates the potential benefits of flying wind-optimal polar routes and assessed their potential impact on climate change. An optimization algorithm is developed for transpolar flights to generate wind-optimal trajectories that minimize climate impact of aircraft, in terms of global warming potentials (relative to warming by one kg of CO₂) of several types of emissions, while avoiding regions of airspace that facilitate persistent contrail formation. Estimations of global warming potential are incorporated into the objective function of the optimization algorithm to assess the climate impact of aircraft emissions discharged at a given location and altitude. The regions of airspace with very low ambient temperature and areas favorable to persistent contrail formation are modeled as undesirable regions that aircraft should avoid and are formulated as soft state constraints. The fuel burn and climate impact of cross-polar air traffic flying various types of trajectory including flight plan, great circle, wind-optimal, and contrail-avoidance are computed for 15 origin-destination pairs between major international airports in the U.S. and Asia. Wind-optimal routes reduce average fuel burn of flight plan routes by 4.4% on December 4, 2010 and 8.0% on August 7, 2010, respectively. The tradeoff between persistent contrail formation and additional global warming potential of aircraft emissions is investigated with and without altitude optimization. Without altitude optimization, the reduction in contrail travel times is gradual with increase in total fuel consumption. When altitude is optimized, a one percent increase in additional global warming potential, a climate impact equivalent to that of 4070kg and 4220kg CO₂ emission, reduces 135 and 105 minutes persistent contrail formation per flight during a day with medium and high contrail formation, respectively.

Introduction

A polar route refers to an aircraft route across the North Polar operations region lying north of 78 deg north latitude [1]. Civilian transpolar flights became possible after the end of the Cold War. Before that, all flights from North America to Asia were routed around the Arctic region due to a buffer zone between the Soviet Union and North America using a series of tracks between Alaska and Japan. The Russian-American Coordinating Group for Air Traffic (RACGAT) was formed in 1993 to coordinate international flights across Russia. Four cross-polar routes were opened in the summer of 1998 with permission from the Russian government. The annual cross-polar operations grew from 402 flights in 2000 to 8527 flights in 2009 [2]. The new polar routes reduce aircraft fuel burn by providing shorter paths between many North American and Asian cities and offer new opportunities for air travel markets. In addition to fuel economy, there is increased urgency to understand and mitigate the impact of air traffic on climate [3]. Greenhouse gases, nitrogen oxides, and contrail generated by air traffic affect the climate in different and uncertain ways. A recent study shows that persistent contrail may have a three to four times greater effect on the climate than carbon dioxide emissions [4]. Flying cross-polar paths can potentially reduce flight times, fuel burn, associated environmental emissions, and climate impact due to contrail formation. These benefits have not been fully utilized because current transpolar flights that transit foreign airspace have limited entry/exit points provide little track flexibility. Air traffic competition for the limited number of tracks can also cause congestion. Flying fixed airways that ignore contrail-favorable regions in airspace and do not make use of prevailing winds or avoid unfavorable winds neglect the benefits of reducing contrails and flying wind-optimal routes. The International Air Transportation Association proposes the establishment of the Pacific Project to meet the increasing air traffic demand between North America and Asia, which is expected

to double by 2025, by promoting seamless airspace between the two regions [5]. As the route structure becomes more flexible and aircraft are allowed to fly their preferred routes, design of optimal aircraft trajectories in winds that minimize fuel consumption and environmental impact are critical factor for the aviation industry to meet their ambitious business and environmental targets.

A recent study examines the travel time and fuel usage savings of transitioning from the fixed Central East Pacific routes to user-preferred routes through develop minimum time wind-optimal routes using dynamic programming algorithm [6]. Several new operational strategies in air traffic management have been proposed that can potentially mitigate the impact of persistent contrail on climate change. These strategies include adjusting cruise altitude [7], [8] and rerouting aircraft around regions of airspace that facilitate persistent contrail formation [9]. Campbell [10] presents a methodology to optimally reroute aircraft trajectories to avoid the formation of persistent contrail with the use of mixed integer programming. Considering the effect of winds, a new study [11] develops a flight trajectory optimization algorithm with fuel and contrail models to compute alternative flight paths that enable tradeoffs between persistent contrail mitigation and fuel consumption. Sridhar [12] develops a hierarchy of simulation models that combines air traffic flow management concepts with both carbon dioxide and non-carbon dioxide emissions for the design of efficient environmentally-aware traffic flow management strategies in the presence of uncertainties. No study has evaluated the potential benefits of flying wind-optimal cross-polar routes and assesses their impact on the climate change. Current objective functions in trajectory optimization algorithms have not incorporated the cost of potential climate impact converted from aircraft fuel consumption and associated emissions.

This study develops optimal aircraft trajectories in winds that minimize climate impact of aircraft, in terms of Global Warming Potentials (GWPs) of several types of emissions while avoiding regions of airspace that facilitate persistent contrail formation. The regions of airspace favorable to persistent contrail formation are modeled as undesirable regions that aircraft should avoid and are formulated as soft state constraints. Similarly, airspace regions that

have atmospheric temperatures below a minimum threshold are undesirable since the FAA requires cross-polar flights to monitor and maintain aircraft fuel above minimum fuel freeze temperatures. The optimal aircraft trajectories are designed by solving a non-linear optimal control problem with path constraints. The dynamical equation for aircraft optimal heading is the solution of the Zermelo problem [13] derived on a spherical Earth surface in the absence of constraints.

The next section explains the aircraft trajectory optimization for cruising aircraft in winds. The Persistent Contrail Formation Section provides the model for diagnosing regions of airspace that are susceptible for persistent contrail formation. The Cold Fuel Management Section introduces background for ensuring unobstructed fuel flow. The Penalty Areas Section models persistent contrail formation areas and airspace with extremely low ambient temperature as regions to be avoided by an aircraft and imposes a soft penalty for going through these regions. The Results Section applies the optimization algorithm to calculate wind-optimal and contrail-avoidance routes for cross-polar flights between 15 major cities in the U.S. and Asia. Conclusions Section presents a summary.

Climate-Impact Minimal Aircraft Trajectory on a Spherical Surface

This section develops the optimal trajectory algorithm that minimizes climate impact of cruising aircraft on a spherical surface. Aircraft trajectory optimization algorithms are well known and are solutions to two-point boundary value problems [13]. The optimal cross-polar aircraft trajectories in this paper are generated by repeatedly computing horizontal trajectories for a range of cruising altitudes. The Horizontal Trajectory Generation Subsection presents the aircraft model and outlines the procedures for calculating optimal aircraft heading on the surface of a sphere. Fuel Consumption and Emissions Subsection models aircraft fuel flow and emissions. Global Warming Potential Subsection introduces the model for the potential impact of aircraft emissions on climate change in terms of GWP.

Horizontal Trajectory Generation

This subsection derives the dynamical equation for optimal aircraft heading. The aircraft equations of motion at a constant altitude h above the spherical Earth's surface are

$$\dot{\phi} = \frac{V \cos \psi + u(\phi, \theta, h)}{R \cos \theta} \quad (1)$$

$$\dot{\theta} = \frac{V \sin \psi + v(\phi, \theta, h)}{R} \quad (2)$$

$$\dot{m} = -f, \quad (3)$$

subject to the conditions that thrust equals drag, flight path angle is zero, and the boundary constraints. ϕ is longitude and θ is latitude, V is airspeed, ψ is heading angle, R is Earth's radius, m is aircraft mass, f is fuel flow rate. The east-component of the wind velocity is $u(\phi, \theta, h)$, and the north-component of the wind velocity is $v(\phi, \theta, h)$. It is assumed that the Earth is a sphere and $R \gg h$.

The horizontal trajectory is optimized by determining the heading angle that minimizes a cost function and satisfies the physical system constraints. The cost function contains components that penalize traveling time, climate impact of aircraft emissions in terms of GWP, and flying through penalty areas. The cost function is defined as

$$J(h) = \int_{t_0}^{t_f} [C_t + \sum_i C_i \cdot GWP_i(\phi, \theta, h) \cdot EI_i \cdot f(h) + C_r r(\phi, \theta, h)] dt, \quad (4)$$

where C_t is the cost coefficient of time, C_i is the cost coefficient of emission i , GWP_i and EI_i are the Global Warming Potential and the Emission Index of trace gas i , respectively, C_r is the cost coefficient of penalty areas, and $r(\phi, \theta, h)$ is the penalty function. The next three subsections discuss the emission index, GWP_i , and penalty function in more detail. The GWP_i and penalty depend on aircraft position and altitude. Fuel flow rate is a constant for a given altitude h . Defining a total risk function of traveling through a penalty area,

$$K(\phi, \theta, h) = \sum_i C_i \cdot GWP_i(\phi, \theta, h) \cdot EI_i \cdot f(h) + C_r r(\phi, \theta, h), \quad (5)$$

the cost function is rewritten as

$$J(h) = \int_{t_0}^{t_f} [C_t + K(\phi, \theta, h)] dt. \quad (6)$$

Pontryagin's Minimum Principle [13] is applied to determine the control input that minimizes the cost function. The heading angle, ψ , is the control available for aircraft during cruise. The Hamiltonian for this problem is defined as

$$H = C_t + K(\phi, \theta, h) + \lambda_\phi \left(\frac{V \cos \psi + u(\phi, \theta, h)}{R \cos \theta} \right) + \lambda_\theta \left(\frac{V \sin \psi + v(\phi, \theta, h)}{R} \right) + \lambda_m (-f) \quad (7)$$

where λ_ϕ , λ_θ , and λ_m are the co-state parameters. The study in [14] determined the value of λ_m to be negligible during cruise portion of flight for transport-class aircraft. The Hamiltonian for the reduced-order model is formulated as

$$H = C_t + K(\phi, \theta, h) + \lambda_\phi \left(\frac{V \cos \psi + u(\phi, \theta, h)}{R \cos \theta} \right) + \lambda_\theta \left(\frac{V \sin \psi + v(\phi, \theta, h)}{R} \right) \quad (8)$$

For an extremum to exist, the optimal heading angle satisfies

$$\frac{\partial H}{\partial \psi} = 0 \Rightarrow \tan \psi = \frac{\lambda_\theta \cos \theta}{\lambda_\phi}, \quad (9)$$

for $t_0 \leq t \leq t_f$, and the necessary condition for optimality is $H^* = 0$ for free arrival-time problem. Solve Eqs. (8, 9) for the co-state parameters λ_ϕ and λ_θ when the Hamiltonian is zero to obtain

$$\lambda_\phi = \frac{-(C_t + K(\phi, \theta, h)) R \cos \psi \cos \theta}{V + u(\phi, \theta, h) \cos \psi + v(\phi, \theta, h) \sin \psi} \quad (10)$$

$$\lambda_\theta = \frac{-(C_t + K(\phi, \theta, h)) R \sin \psi}{V + u(\phi, \theta, h) \cos \psi + v(\phi, \theta, h) \sin \psi}. \quad (11)$$

The co-state equations are

$$\begin{aligned} -\dot{\lambda}_\phi &= \frac{\partial H}{\partial \phi} \\ &= \frac{\partial K(\phi, \theta, h)}{\partial \phi} + \frac{\lambda_\phi}{R \cos \theta} \left(\frac{\partial u(\phi, \theta, h)}{\partial \phi} \right) + \frac{\lambda_\theta}{R} \left(\frac{\partial v(\phi, \theta, h)}{\partial \phi} \right), \end{aligned} \quad (12)$$

$$\begin{aligned} -\dot{\lambda}_\theta &= \frac{\partial H}{\partial \theta} \\ &= \frac{\partial K(\phi, \theta, h)}{\partial \theta} + \frac{\lambda_\phi}{R \cos \theta} \left(\frac{\partial u(\phi, \theta, h)}{\partial \theta} \right) \\ &\quad + \frac{\lambda_\phi \tan \theta (V \cos \psi + u(\phi, \theta, h))}{R \cos \theta} + \frac{\lambda_\theta}{R} \left(\frac{\partial v(\phi, \theta, h)}{\partial \theta} \right). \end{aligned} \quad (13)$$

Equations (9, 12, 13) are known as the Euler-Lagrange equations. Differentiate both sides of Eq. (9) with respect to time, and substitute Eqs (10-13) to obtain the dynamical equation for the optimal aircraft heading,

$$\dot{\psi} = \frac{-[F_{\text{wind}}(\psi, \phi, \theta, u, v) + F_{\text{climate}}(\psi, \phi, \theta, u, v, K)]}{R \cos \theta (C_t + K(\phi, \theta, h))}, \quad (14)$$

where $F_{\text{wind}}(\psi, \phi, \theta, u, v)$ and $F_{\text{climate}}(\psi, \phi, \theta, u, v, K)$ are aircraft heading dynamics in response to winds and climate impact, respectively. Their expressions are shown in the Appendix. Note that the two-point boundary value problem is reduced to an initial value problem that will be solved using a collocation method to calculate the optimal initial aircraft heading. Integrate Eqs. (1, 2, 14) simultaneously using the initial aircraft position and the optimal heading to obtain the optimal trajectory in the presence of winds and minimizing travel through penalty regions.

Fuel Consumption and Emission Models

This study applies the fuel consumption model in Eurocontrol's Base of Aircraft Data Revision 3.6 (BADA) [15] to compute cruising aircraft fuel consumption. The fuel burn for aircraft during cruise, f , is calculated as

$$f = t \cdot SFC \cdot Th, \quad (15)$$

where t is elapsed time, Th is thrust, and SFC is the specific fuel consumption.

The emission model is based on the System for assessing Aviation's Global Emissions (SAGE) developed by the Federal Aviation Administration (FAA) [16]. Six emissions are computed including CO_2 , H_2O , SO_x , CO , HC and NO_x . Emissions of CO_2 , H_2O and SO_x (modeled as SO_2) are directly proportional to fuel consumption [17]. The emissions are computed by

$$\begin{aligned} E_{\text{CO}_2} &= EI_{\text{CO}_2} \cdot f = 3155 \cdot f, \\ E_{\text{H}_2\text{O}} &= EI_{\text{H}_2\text{O}} \cdot f = 1237 \cdot f, \\ E_{\text{SO}_2} &= EI_{\text{SO}_2} \cdot f = 0.8 \cdot f. \end{aligned} \quad (16)$$

The terms E_{CO_2} , EI_{CO_2} , $E_{\text{H}_2\text{O}}$, $EI_{\text{H}_2\text{O}}$ and E_{SO_2} , EI_{SO_2} are emissions and emission index of CO_2 , H_2O and SO_2 . The emissions are in grams, and fuel burns are in kilograms.

Emissions of CO , HC and NO_x are modeled through the use of the Boeing Fuel Flow Method 2 (BFFM2) [18]. The emissions are determined by aircraft engine type, altitude, speed, and fuel burn and the coefficients in the International Civil Aviation Organization (ICAO) emission data bank. They are in grams and computed by

$$\begin{aligned} E_{\text{CO}} &= EI_{\text{CO}} \cdot f, \\ E_{\text{HC}} &= EI_{\text{HC}} \cdot f, \\ E_{\text{NO}_x} &= EI_{\text{NO}_x} \cdot f. \end{aligned} \quad (17)$$

In the models, fuel burn is corrected to sea-level reference temperature, θ_{amb} , and pressure, δ_{amb} by the following equations:

$$\begin{aligned} f_c &= (f / \delta_{\text{amb}}) [\theta_{\text{amb}}^{3.8} e^{0.2 \cdot M^2}], \\ \delta_{\text{amb}} &= P_{\text{amb}} / 14.696, \\ \theta_{\text{amb}} &= (T_{\text{amb}} + 273.15) / 273.15, \end{aligned} \quad (18)$$

where f_c is the corrected fuel flow, P_{amb} is the at-altitude ambient pressure, T_{amb} is the at-altitude ambient temperature, and M is the Mach number. f_c is used in ICAO emission data bank to determine the reference emission index REI_{HC} , REI_{CO} and REI_{NO_x} for HC , CO and NO_x . The emission indices are computed by

$$\begin{aligned} EI_{\text{CO}} &= REI_{\text{CO}} (\theta_{\text{amb}}^{3.3} / \delta_{\text{amb}}^{1.02}), \\ EI_{\text{HC}} &= REI_{\text{HC}} (\theta_{\text{amb}}^{3.3} / \delta_{\text{amb}}^{1.02}), \\ EI_{\text{NO}_x} &= REI_{\text{NO}_x} \cdot e^H \cdot (\delta_{\text{amb}}^{1.02} / \theta_{\text{amb}}^{3.3})^{0.5}, \\ H &= -19.0(\omega - 0.0063). \end{aligned} \quad (19)$$

EI_{CO} , EI_{HC} and EI_{NO_x} are emission indices of CO , HC and NO_x , H is the humidity correction factor, and ω is the specific humidity.

Global Warming Potential

Climate impact of aircraft emissions depends on the quantity, lifetime, and discharged location of each trace gas. A simple climate assessment model accounting for these conditions evaluates the impact in terms of global warming potentials [19]. This model is employed in the trajectory optimization for translating various aircraft emissions into total effect on global warming.

The GWP for a type of emission is the ratio of the global warming through emission of 1 kg of the gas to the global warming through emission of 1 kg of CO₂:

$$GWP_i(T) = \frac{E_i(T)}{E_{CO_2}(T)} \quad (20)$$

where T is the time horizon and E_i is the warming effect of the trace gas i . Integrating the radiative forcing RF_i of the trace gas in the time horizon to calculate the warming effect

$$E_i(T) = \int_0^T RF_i \cdot e^{-t/\tau_i} dt = RF_i \cdot \tau_i \cdot (1 - e^{-T/\tau_i}), \quad (21)$$

where τ_i is the life time of the trace gas. GWP varies with the time horizon chosen. The time horizon of 100 years is chosen in this study.

This study only considers the GWP for CO₂, H₂O, and NOx emissions because the amount of CO, HC, and SO₂ emissions per unit of fuel burn is very small. The CO₂, H₂O, and NOx emissions are converted into GWP figures using conversion factors shown in Appendix, Table A.1 adopted from Svensson [19]. The conversion for H₂O or NOx emission depends on altitude only while GWP of CO₂ is completely independent of emitted position. The cost due to global warming potential of aircraft emissions in the cost function is reduced to

$$J_{GWP}(h) = \int_{t_0}^{t_f} \left[\sum_i C_i \cdot GWP_i(h) \cdot EI_i \cdot f(h) \right] dt, \quad (22)$$

and the rate of change in the total risk function with respect to aircraft position, i.e. Eq. (A3) becomes

$$\begin{aligned} \frac{\partial K(\phi, \theta, h)}{\partial \phi} &= C_r \frac{\partial r(\phi, \theta, h)}{\partial \phi}, \\ \frac{\partial K(\phi, \theta, h)}{\partial \theta} &= C_r \frac{\partial r(\phi, \theta, h)}{\partial \theta}. \end{aligned} \quad (23)$$

In the absent of penalty areas (i.e., $C_r = 0$), each horizontal optimal trajectory minimizes the total GWP of CO₂, H₂O, and NOx emissions for a specific cruising altitude. When cruising altitude is optimized, the optimal trajectory is obtained by selecting the flight altitude that yields the minimum GWP trajectory among all possible cruising altitudes.

Persistent Contrail Formation

Besides climate impact of aircraft emissions, persistent contrails may have a greater effect on the climate than carbon dioxide emissions. The formation of contrails has been under investigation since 1919 [20]. According to Appleman [21], contrail are clouds that form when a mixture of warm engine exhaust gases and cold ambient air reaches saturation with respect to water, forming liquid drops, which quickly freeze. Contrails form in the regions of airspace that have ambient Relative Humidity with respect to Water (RH_w) greater than a critical value, r_{contr} [22]. Contrails can persist when the ambient air is supersaturated with respect to ice, i.e. the environmental Relative Humidity with respect to Ice (RH_i) is greater than 100% [23]. In this study, the regions of airspace that have RH_w greater than r_{contr} and RH_i greater than 100% are considered favorable to persistent contrail formation. Degrand [24] and Palikonda [25] measure the validity of contrail formation by comparing them with satellite observation. There is general agreement between the satellite images and the persistent contrail regions predicted by the model.

The estimated critical relative humidity r_{contr} for contrail formation at a given temperature T (in degrees Celsius) can be calculated as [22]

$$r_{contr} = \frac{G(T - T_{contr}) + e_{sat}^{liq}(T_{contr})}{e_{sat}^{liq}(T)}, \quad (24)$$

where $e_{sat}^{liq}(T)$ is the saturation vapor pressure over water at a given temperature. The estimated threshold temperature (in degrees Celsius) for contrail formation at liquid saturation is [20]

$$T_{contr} = -46.46 + 9.43 \ln(G - 0.053) + 0.72 [\ln(G - 0.053)]^2, \quad (25)$$

where $G = \frac{EI_{H_2O}C_pP}{\varepsilon Q(1-\eta)}$. EI_{H_2O} is the emission index of water vapor, and it is assumed to be 1.25;

$C_p = 1004 \text{ J kg}^{-1} \text{ K}^{-1}$ is the isobaric heat capacity of air, P (in Pa) is the ambient air pressure, $\varepsilon = 0.6222$ is the ratio of molecular masses of water and dry air, $Q = 43 \times 10^6 \text{ J kg}^{-1}$ is the specific combustion heat, and $\eta = 0.3$ is the average propulsion efficiency of the jet engine.

The values of r_{contr} and RHi are computed using measurements from the Global Forecast System (GFS). GFS is a global numerical weather prediction computer model run by the National Oceanic & Atmospheric Administration (NOAA) four times a day. It produces a forecast for every 3rd hour for the first 180 hours, and after that, every 12 hours up to 16 days. The horizontal resolution is roughly equivalent to 0.5X0.5 degree latitude/longitude. GFS data have 64 unequally-spaced vertical isobaric pressure levels ranging between 0.25-1000 mb with enhanced resolution near the bottom and the top. The value of r_{contr} is computed by Eqs. (24, 25) using GFS measurements for RHw and temperatures. GFS does not provide measurements for RHi directly. Instead, RHi is calculated by the following formula:

$$RHi = RHw \cdot \frac{6.0612 e^{18.102 \cdot T / (249.52 + T)}}{6.1162 e^{22.577 \cdot T / (273.78 + T)}}. \quad (26)$$

Note that the numerator on the right hand side of Eq. (26) is the saturation vapor pressure over water $e_{sat}^{liq}(T)$ from the model denoted as AERW(50, -80) in Alduchov's study [26] and the denominator is the saturation vapor pressure over ice from the model denoted as AERWi(0, -80) in Alduchov's study [26]. This study identifies the airspace regions favorable to persistent contrail formation using Eq. (24-26) and weather data from GFS.

Cold Fuel Management

This study models the airspace regions with ambient temperature below 208 °K (-65 °C) [27] as penalty areas to reduce the risk of fuel freezing. Aircraft fuel temperature may approach the freezing point for cross-polar flights due to the long flight duration inside regions with extremely low temperature. The maximum freezing point for jet fuel depends on the geographical region of the fuel supply. Past data show that the average freezing point of delivered Jet A fuel at the U.S. airports is

between -43°C and -50°C [1]. The pour point is defined as the lowest temperature at which the fuel still flows. It is the critical condition of cold fuel, and is approximately 6°C lower than the freezing point.

The fuel temperature for long flights tends to adjust to the temperature of the aerodynamic boundary layer over the wing skin. This temperature is slightly lower than the Total Air Temperature (TAT) that is higher than the ambient air temperature. The flight crew must increase the TAT when the fuel temperature drops to 3°C above the freezing point to avoid further cooling of the fuel.

Cross-polar flights change the flight plan or flight level to airspace with warmer ambient air, if necessary, to ensure unobstructed fuel flow. Increasing aircraft speed also increase TAT. These actions lead to more fuel consumption. This study models the airspace regions with very low ambient temperature as penalty areas during the flight path planning to minimize the risk of fuel freezing and additional fuel burn associated with the correcting actions.

Penalty Areas

Persistent contrail-favorable regions are modeled using penalty functions as areas to be avoided by an aircraft to reduce the potential impact on climate. The penalty functions enable a systematic way of generating aircraft trajectories that avoid the contrail formation areas by varying amounts. The airspace regions have ambient temperature below 208°K are also identified using GFS data and modeled as penalty areas for managing fuel temperature. The cost due to persistent contrail formation and cold fuel risk is defined as

$$\begin{aligned} J_r(h) &= \int_{t_0}^{t_f} C_r r(\phi, \theta, h) dt \\ &= \int_{t_0}^{t_f} [C_r^C r_{Contrail}(\phi, \theta, h) + C_r^F r_{Freeze}(\phi, \theta, h)] dt. \end{aligned} \quad (27)$$

The penalty function $r(\phi, \theta, h)$ provides the penalties that an aircraft can encounter along the flight trajectory from the origin to destination. In general, there are multiple regions in the en-route airspace that favor persistent contrail formation or have extremely low ambient temperature. The penalty is determined by the radial penalty function-

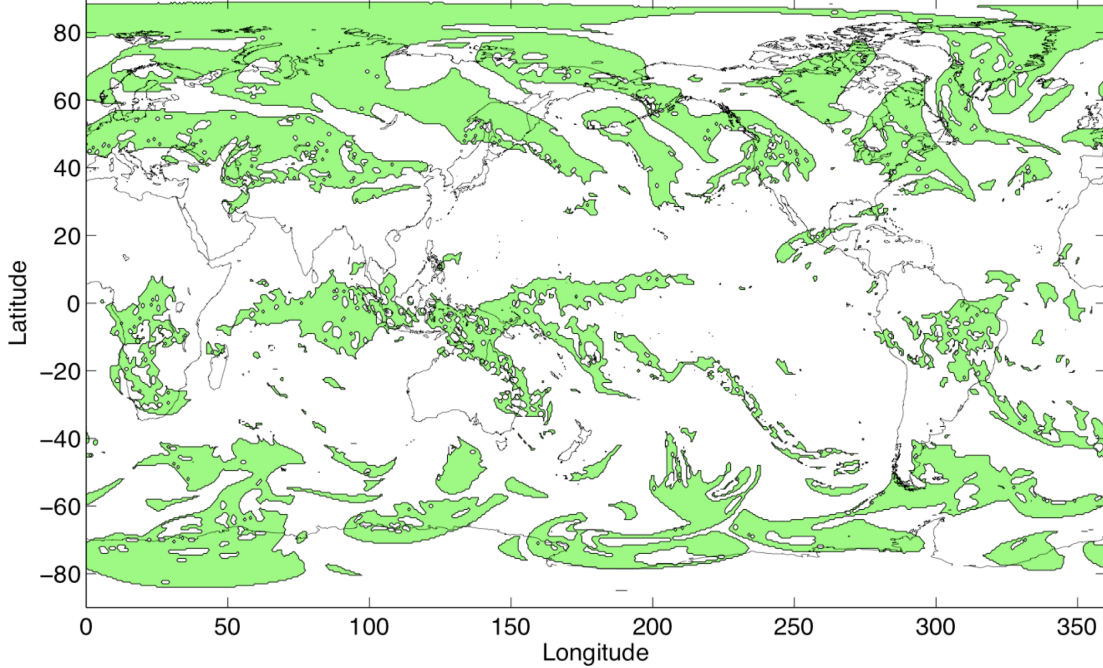


Figure 1. Persistent Contrails Favorable Regions at 8 p.m. EDT on December 31, 2009

$$r_{Contrail}(\phi, \theta, h) = \sum_i \frac{1}{(d_i^C)^2}, \quad (28)$$

$$r_{Freeze}(\phi, \theta, h) = \sum_i \frac{1}{(d_i^F)^2},$$

where d_i^C and d_i^F are distances between the aircraft and the center of i^{th} region that potentially form persistent contrails and has ambient temperature below 208°K , respectively. The penalty coefficients C_r^C and C_r^F are treated as design parameters. The choice of these parameters is not unique and depends on the definition of the penalty function itself. In addition, there are many regions in the NAS that can potentially form persistent contrails. Some are far away from the aircraft and will not be encountered by the aircraft. Some regions are too large for aircraft to completely avoid. Identifying the right subset of contrail and avoiding the region by an appropriate level are important for policy makers to make decisions and tradeoffs. Note that the GWP conversions for persistent contrail formation are not modeled currently. The climate impact due to contrails is assessed by investigating the time

associated traveling through regions of persistent contrail formation.

This study chooses a larger magnitude for C_r^F than that of C_r^C to reflect a higher priority for avoiding low temperature regions. Maneuvering aircraft away from these areas horizontally should not be mistaken as the primary strategy for managing fuel temperature since there are other efficient alternatives such as adjusting altitude or speed.

Results

This section applies the optimal trajectory algorithm to calculate trajectories for cross-polar flights and evaluates their potential impacts to the climate change in terms of global warming potential of aircraft emissions and the time associated traveling through regions of persistent contrail formation. The trajectory computations are done using several days of U.S. to Asia traffic data for 2007 and 2010 and global atmospheric data for 2009 and 2010. The data for temperature, RHw, wind speed and direction are obtained from GFS. The filled green polygons in Fig. 1 depict the areas at 30,000 feet above sea level around the world where atmospheric conditions were

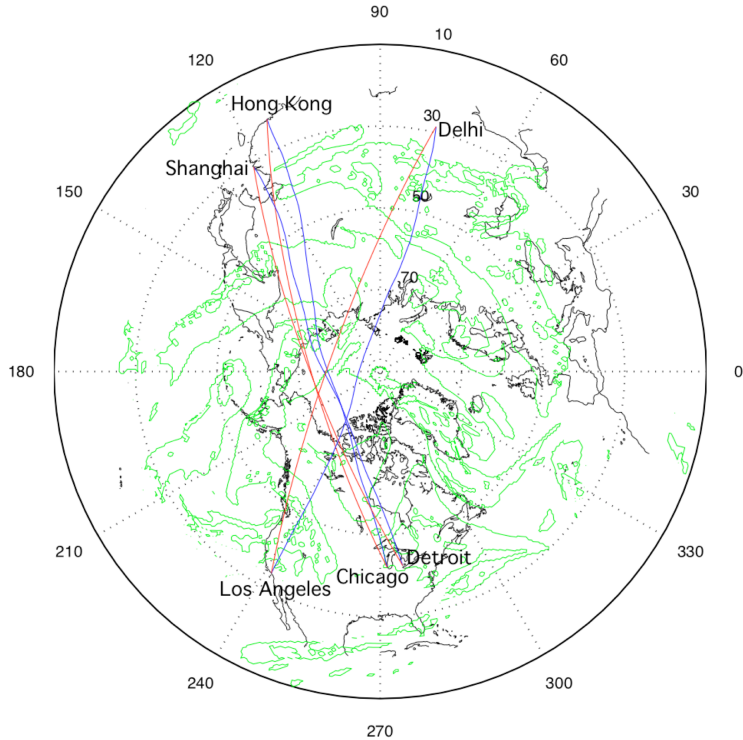


Figure 2. Cross-polar Trajectories from U.S. to Asia for 3 City Pairs and Contrails Favorable Regions

favorable for persistent contrail formation at 8 p.m. EDT on December 31, 2009. The critical relative humidity and RH_i values are computed using Eq. (24-26).

The next subsection analyzes Great Circle (GC) and Wind Optimal (WO) trajectories for three cross-polar flights from U.S. to Asia. Then, four cross-polar trajectory designs from Chicago O'Hare to Hong Kong are evaluated. The last subsection presents results for 15 Origin-Destination (OD) pairs.

Great Circle and Wind Optimal Trajectories

This subsection analyzes the GC and WO trajectories for 3 cross-polar flights from Chicago to Hong Kong, Los Angeles to New Delhi, and Detroit to Shanghai on December 31, 2009. Figure 2 plots the GC trajectories in red and WO trajectories in blue for each city pair. The aircraft is at 30,000 feet with a speed of 490 knots (907 km/hr), a typical cruising speed for a Boeing 777-200. The areas favorable to persistent contrail formation are surrounded by the green polygons. The atmospheric conditions including wind data are obtained from GFS, at 8 p.m.

EDT that day. The WO trajectory is generated using Eqs. (1, 2, 14) by setting $C_r = 0$. The performance of optimal trajectories is evaluated by investigating the fuel consumption, aircraft emissions, GWP, and the time associated traveling through regions of persistent contrail formation.

Table 1 shows the performance data for the cross-polar trajectories. The aircraft fuel burn and emissions are computed using Eq. (15-19). The WO trajectories have about 0.3% to 2% fuel savings when compared to the GC trajectories. The CO₂, H₂O, and NOx emissions are 2-5 order of magnitude larger than SO_x, CO and HC emissions. The CO₂, H₂O, and NOx emissions are converted into GWP figures using Table A.1. The total GWP for each trajectory is shown in Table 1. The GWP of H₂O, and NOx emissions are about 50% of the GWP figure for CO₂ alone, thus their impacts on climate are not negligible. The GWP for these trajectories are equivalent to the global warming effect through emission of 472-525 metric ton of CO₂. The total minutes that aircraft travel inside contrail-favorable regions are provided since the GWP conversions for persistent contrail formation are not modeled

Table1. Potential Climate Impact of Great Circle and Wind-Optimal Trajectories

OD Pairs	ORD/HKG		LAX/DEL		DTW/PVG	
Trajectory	GC	WO	GC	WO	GC	WO
Fuel (ton)	110	108	107	106	99.6	99.3
CO ₂ (ton)	348	341	338	337	314	313
H ₂ O (ton)	136	134	133	132	123	123
NO _x (ton)	2.63	2.58	2.56	2.55	2.37	2.37
SO _x (ton)	0.09	0.09	0.09	0.09	0.08	0.08
CO (ton)	0.05	0.05	0.05	0.05	0.04	0.04
HC (ton)	0.01	0.01	0.01	0.01	0.01	0.01
GWP	525	515	510	508	473	472
Contrail (minutes)	319	377	333	345	512	300

currently. Flying WO trajectories for the three OD pairs results in GWP savings equivalent to reducing 13 ton of CO₂ emissions and a potential reduction of 142 minutes of persistent contrail formations.

Chicago to Hong Kong

The trajectory design in this example focuses on minimizing the total GWP of aircraft emissions and avoiding the potential contrail regions between Chicago and Hong Kong. The total GWP of aircraft emissions, the time through contrail regions, and the minimum environmental temperature en-route are computed for each trajectory. This process is

repeated at all the six possible flight levels 300, 320, 340, 360, 380, 400. Four trajectories from Chicago O'Hare international airport (ORD) to Hong Kong international airport (HKG) are shown in Fig. 3 for cross-polar flights with cruising altitude and speed equal to 32,000 feet and 490 knots (907 km/hr), respectively. The green polygons outline the regions that are favorable to persistent contrail formation at 12 a.m. EDT on January 1, 2010. The GC trajectory is plotted in red-dashed line; and WO trajectory, actual Flight Plan (FP), and partial Contrail Avoidance (CA) trajectory are plotted in blue, red and magenta solid lines, respectively.

Optimal aircraft trajectories are generated for 6 different altitudes between 30,000 feet and 40,000 feet. This study assumes that the cruising altitudes are between 30,000 and 40,000 feet; and eastbound aircraft fly odd thousands of feet while westbound aircraft fly even thousands of feet. At each altitude, the cost coefficient of time is chosen as $C_t = 20$; the coefficient for low temperature areas is $C_r^F = 1$; and C_r^C is varied from 0 to 1 in increments of 0.1 to generate a collection of contrail-avoidance trajectories.

The upper part of Fig. 4 shows the GWP for the trajectories on six flight levels, and the lower part shows total time that aircraft travel inside the regions of airspace favorable to persistent contrail formation. The WO trajectories have the smallest GWP at all flight levels, and have 13,000-106,000 unit of GWP savings when compared to the flight plan routes. GC routes have smaller GWP than the flight plan routes except at flight level 300. Flying GC trajectories do not always lead to a smaller GWP figures in the

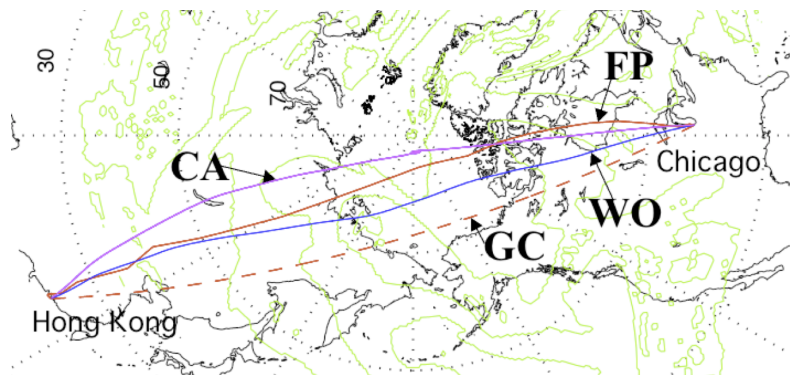


Figure 3. Aircraft Trajectories at 32,000 Feet from Chicago to Hong Kong with Different Design Parameters

presence of winds. In this example, aircraft flying at higher altitudes produce smaller GWP. The trajectories at flight level 400 do not intercept any region of airspace that facilitates persistent contrail formation. When altitude is optimized, aircraft should fly the WO trajectories at this cruising altitude that minimize total GWP and contrails.

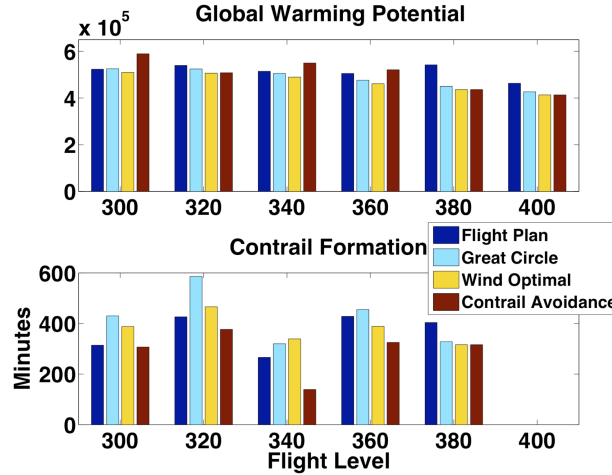


Figure 4. Global Warming Potential and Total Travel Time Inside Contrail Favorable Regions

Flying wind optimal routes at other flight levels potentially cause persistent contrail formation. Contrail avoidance trajectory is the same as the WO trajectory at flight level 380 since the current C_r values do not result in trajectories that reduce contrail formation. More optimal trajectories can be calculated with various choices of C_r . Flying the CA trajectories produce additional 79,000, 1,000, 60,000, and 60,000 units of GWP at flight level 300, 320, 340, and 360, respectively, to avoid potentially 81, 89, 200, and 64 minutes of persistent contrail formation when compared to the WO trajectories. There is a tradeoff between flying a route that produces smaller GWP with more persistent contrail formation versus flying a route that generates larger GWP with less persistent contrail formation. The next subsection presents more results for optimal trajectory selections based on the tradeoff between GWP reduction and Contrail formation. Table 2 shows the minimum atmosphere temperature along the flight trajectories at each flight levels. The temperatures decrease as flight level increases. Aircraft can operate safely in this case since the minimum atmosphere temperature is above 208 °K (-65 °C).

Table 2. Minimum Atmosphere Temperature (K)

Trajectory	Flight Level					
	300	320	340	360	380	400
Flight Plan	242	236	230	225	219	215
Great Circle	241	236	230	225	220	216
Wind Optimal	241	236	230	225	220	216
Contrail Avoidance	241	236	230	225	220	216

Optimal Trajectories for 15 Origin-Destination Pairs

This subsection analyzes the FP, GC, WO, and CA trajectories for cross-polar flights between the 15 OD pairs as listed in Table 3. Cross-polar flights are currently flying almost daily between these major international airports. First, simulating GC trajectories to assess the severity of potential contrail formation induced by cross-polar air traffic throughout the year of 2010. The results identify the days in 2010 that have medium and high potential contrail formation for the 15 OD pairs. Then, climate impact of cross-polar air traffic is investigated in more detail for these days.

Persistent contrail-favorable regions around the world are identified for the first week in each month in 2010 using atmospheric data from the GFS. The total time that aircraft fly inside contrail-favorable regions are recorded each day for GC trajectories at flight levels 300, 340 and 380, respectively. Figure 5 shows the average contrail formation time for the first week of each month in 2010. The yearly average is 203 minutes per flight. August 7 has medium (195 minutes) contrail formation and December 4 has the highest (370 minutes) contrail formation. In general, contrail formation tends to be more severe during winter than summer.

The FP, GC, WO, and CA trajectories are simulated using air traffic data on August 4-7, 2010 and atmospheric data on August 7 and December 4, 2010. Airspace regions around the world that have ambient temperature below 208°K (-65°C) are identified for August 7 and December 4, 2010 in addition to the contrail favorable regions. This study assumes that the cruising altitudes remain constant at even flight levels between 300 and 400 since most

cross-polar flights are west-bound except the OD from Los Angeles to Dubai.

Table 3. Selected International Airport Pairs

	Origin to Destination
1	John F. Kennedy – Seoul Incheon
2	John F. Kennedy – Hong Kong
3	John F. Kennedy – Beijing Capital
4	Newark Liberty – Singapore Changi
5	Newark Liberty – Hong Kong
6	Newark Liberty – Shanghai Pudong
7	Chicago O’Hare – Seoul Incheon
8	Chicago O’Hare – Hong Kong
9	Chicago O’Hare – Beijing Capital
10	Chicago O’Hare – Shanghai Pudong
11	Washington Dulles – Seoul Incheon
12	Washington Dulles – Beijing Capital
13	Washington Dulles – Narita
14	Hartsfield-Jackson Atlanta – Seoul Incheon
15	Los Angeles – Dubai

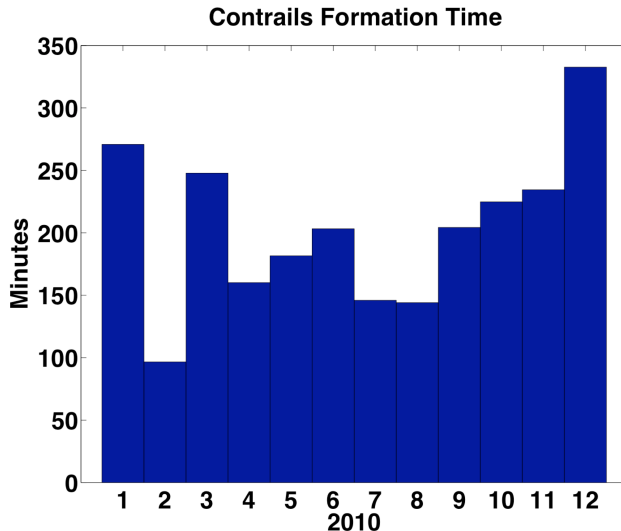


Figure 5. Contrail Formation Time in 2010

The FP, GC, and WO optimal aircraft trajectories are generated at the departure time at six

flight levels for each OD pair. In addition, a group of 10 CA trajectories are calculated for each flight level by increasing the value of C_r^C from 0 to 1 with increments of 0.1. The cost coefficient of time is chosen as $C_t = 20$ and $C_r^F = 1$ for each case. The cruising speed is assumed to be 490 knots.

Table 4. Average Cross-polar Trajectories Performance for the 15 City Pairs

		Fuel Burn (ton)	GWP (1000)	Fuel Savings (%)
8/7/10	FP	91.7	442	0.0
	GC	89.1	430	2.8
	WO	84.4	407	8.0
12/4/10	FP	91.4	441	0.0
	GC	89.3	431	2.3
	WO	87.4	422	4.4

Flying WO and GC trajectories reduce average fuel consumption significantly when compared to that of FP routes. The average fuel burn and GWP for the three trajectory types, and average fuel savings over FP is presented in Table 4. Note that the fuel savings is equivalent to the GWP savings when cruising altitude is not optimized. WO trajectories reduce average fuel burn (GWP) by 4.4% on December 4, 2010 and 8.0% on August 7, 2010, respectively. Note that no computed trajectories fly inside airspace with temperature below the threshold. These low temperature regions are very small during summer. The cross-polar flights did not encounter the low temperature regions for the selected winter day.

In the CA trajectory group, the additional GWP of each optimal trajectory is obtained by comparing its GWP figure to that of its wind-optimal trajectory. The persistent contrail formation time associated with each trajectory is also recorded. A total of five bins are defined such that the aircraft trajectories can be categorized based on their additional GWP production. These are presented in Fig. 6. The first bin contains the wind-optimal trajectory, which is the baseline for GWP comparison and corresponds to trajectories that producing 0% of additional GWP.

The second bin contains aircraft trajectories that produce less than 1% additional GWP, the third bin contains those producing less than 2%, etc. Note that there are five bins for each group of trajectories designed with various C_r^C values and six groups per flight that each corresponds to one of the six flight levels.

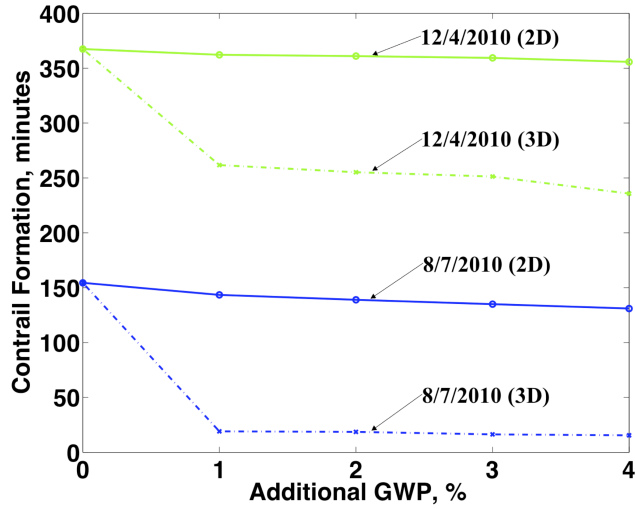


Figure 6. Trade-off Curves Between GWP and Contrail Avoidance

These optimal trajectories consume different amounts of additional fuel and have different GWP values at each bin. In general, the flights, which can afford more additional fuel burn and GWP, induce fewer contrails since they have more routes to choose from. The flights, which can select the flying altitudes, induce much fewer contrails given the same amount of extra fuel.

Figure 6 shows the trade-off curves with (solid curve) and without (dash-dot curve) altitude optimization for a summer (blue curve) day and a winter (green curve) day, respectively. The figure shows, when altitude is optimized, a one percent increase in total GWP production can reduce the total travel times through contrail regions from 154 minutes to 19 minutes during an average contrail day and from 367 minutes to 262 minutes during a high contrail day. Allowing further increase in GWP production does not result in proportionate reduction in contrail travel times. Without altitude optimization, the reduction in contrail travel times is gradual with increase in total fuel consumption.

A tradeoff curve for total minutes through the contrail regions versus extra fuel consumption can be produced similarly. Without altitude optimization, this curve is the same as the solid curve in Figure 6. With altitude optimization, the fuel tradeoff curve is not the same as GWP tradeoff curve since emissions have different climate impact at each altitude. However, the trend of contrail reduction remains very similar for to the GWP tradeoff curve.

The data in Table 4 and Figure 6 can be extended to determine the optimal routes that minimize total climate impact of cross-polar air traffic. For example, CA trajectories producing 1% additional GWP on August 7 have an additional climate impact equivalent to that of 4070kg of CO₂ emission. They reduce an average of 135 minutes persistent contrail formation per flight. When climate impact of contrail in relation to CO₂ emission is known, total climate impact of cross-polar air traffic can be minimized.

Conclusion

An algorithm was developed in this study to calculate wind-optimal trajectories for cross-polar flights while avoiding the regions of airspace that facilitate persistent contrail formation or have very low ambient temperature. The operational strategies investigated for minimizing aviation impact on climate change, in terms of global warming potential, include flying great circle, wind-optimal routes, avoiding partial persistent contrail formation and altering cruising altitudes. The fuel burn and climate impact of cross-polar air traffic flying various types of trajectory are assessed for 15 origin-destination pairs between major international airport in the U.S. and Asia. Persistent contrail favorable regions around the world are identified for the first week in each month in 2010. The yearly average is 203 minutes per flight. August 7 has medium (195 minutes) contrail formation and December 4 has the highest (370 minutes) contrail formation. In general, contrail formation tends to be more severe during winter than summer. Wind-optimal routes reduce average fuel burn of flight plan routes by 4.4% on December 4, 2010 and 8.0% on August 7, 2010, respectively. The tradeoff between persistent contrail formation and additional global warming potential of aircraft emissions is investigated with and without altitude optimization. Without altitude optimization, the reduction in contrail travel times is gradual with

increase in total fuel consumption. When altitude is optimized, a one percent increase in additional global warming potential, a climate impact equivalent to that of 4070kg and 4220kg of CO₂ emission, reduce 135 and 105 minutes persistent contrail formation per flight during a day with medium and high contrail formation, respectively. Further increase in GWP does not significantly reduce contrail formation times.

Future work will model the climate impact of persistent contrail formation in relation to CO₂ emission to minimize total climate impact of cross-polar air traffic.

Appendix

The aircraft heading dynamics in response to winds $F_{\text{climate}}(\psi, \phi, \theta, u, v, K)$ and climate impact $F_{\text{wind}}(\psi, \phi, \theta, u, v)$ are expressed as the following:

$$\begin{aligned}
 & F_{\text{climate}}(\psi, \phi, \theta, u, v, K) \\
 &= [\sin \psi \cos \psi \sin \theta v(\phi, \theta, h) K(\phi, \theta, h) \\
 &+ \cos \theta \cos \psi \sin \psi \frac{\partial v(\phi, \theta, h)}{\partial \theta} K(\phi, \theta, h) \\
 &- \cos \theta \cos \psi \sin \psi v(\phi, \theta, h) \frac{\partial K(\phi, \theta, h)}{\partial \theta} \\
 &+ V \cos \psi \sin \theta K(\phi, \theta, h) + V \sin \psi \frac{\partial K(\phi, \theta, h)}{\partial \phi} \\
 &- \frac{\partial v(\phi, \theta, h)}{\partial \phi} K(\phi, \theta, h) + v(\phi, \theta, h) \frac{\partial K(\phi, \theta, h)}{\partial \phi} \\
 &- \sin \psi \cos \psi \frac{\partial u(\phi, \theta, h)}{\partial \phi} K(\phi, \theta, h) \\
 &+ \sin \psi \cos \psi u(\phi, \theta, h) \frac{\partial K(\phi, \theta, h)}{\partial \phi} \\
 &+ \cos^2 \psi \sin \theta u(\phi, \theta, h) K(\phi, \theta, h) \\
 &+ \cos^2 \psi \cos \theta \frac{\partial u(\phi, \theta, h)}{\partial \theta} K(\phi, \theta, h) \\
 &- V \cos \theta \cos \psi \frac{\partial K(\phi, \theta, h)}{\partial \theta} \\
 &- \cos \theta \cos^2 \psi u(\phi, \theta, h) \frac{\partial K(\phi, \theta, h)}{\partial \theta} \\
 &+ \cos^2 \psi \frac{\partial v(\phi, \theta, h)}{\partial \phi} K(\phi, \theta, h) \\
 &- \cos^2 \psi v(\phi, \theta, h) \frac{\partial K(\phi, \theta, h)}{\partial \phi}], \tag{A1}
 \end{aligned}$$

$$\begin{aligned}
 & F_{\text{wind}}(\psi, \phi, \theta, u, v) \\
 &= [-C_t \sin \psi \cos \psi \frac{\partial u(\phi, \theta, h)}{\partial \phi} \\
 &+ C_t \cos^2 \psi \sin \theta u(\phi, \theta, h) \\
 &+ C_t \cos^2 \psi \cos \theta \frac{\partial u(\phi, \theta, h)}{\partial \theta} - C_t \frac{\partial v(\phi, \theta, h)}{\partial \phi} \\
 &+ C_t \sin \psi \cos \psi \sin \theta v(\phi, \theta, h) \\
 &+ C_t \cos \psi \sin \psi \cos \theta \frac{\partial v(\phi, \theta, h)}{\partial \theta} \\
 &+ C_t V \cos \psi \sin \theta + C_t \cos^2 \psi \frac{\partial v(\phi, \theta, h)}{\partial \phi}], \\
 & \tag{A2}
 \end{aligned}$$

where

$$\begin{aligned}
 \frac{\partial K(\phi, \theta, h)}{\partial \phi} &= \sum_i C_i \cdot \frac{\partial GWP_i(\phi, \theta, h)}{\partial \phi} \cdot EI_i \cdot f(h) \\
 &+ C_r \frac{\partial r(\phi, \theta, h)}{\partial \phi}, \text{ and} \\
 \frac{\partial K(\phi, \theta, h)}{\partial \theta} &= \sum_i C_i \cdot \frac{\partial GWP_i(\phi, \theta, h)}{\partial \theta} \cdot EI_i \cdot f(h) \\
 &+ C_r \frac{\partial r(\phi, \theta, h)}{\partial \theta}. \tag{A3}
 \end{aligned}$$

The dynamical equations (A1, A2) are derived using computer software, and they can be rewritten in a more compact form. Note that Equation A1 is the solution of the Zermelo problem [13] solved in the spherical coordinates.

Table A.1 GWP Figures for CO₂, H₂O and NO_x at Various Flight Levels

Flight Level	CO ₂	H ₂ O	NO _x
300	1	0.04	65.3
320	1	0.18	67.9
340	1	0.28	64.8
360	1	0.34	58.0
380	1	0.39	51.1
400	1	0.45	42.4

References

- [1] Polar Route Operations, Aero, 16, Boeing, http://www.boeing.com/commerical/aeromagazine/ae_ro_16/polar_route_ops.pdf.

- [2] UAL Update Presentation, "Polar Operations 1996 to 2010," 10th Meeting of the Cross Polar Trans-East ATM Providers' Working Group, Paris, France, November 2010.
- [3] "Aviation and the Global Atmosphere," Technical Report, IPCC's Working Groups, London, UK, 2000.
- [4] Waitz, I., J. Townsend, J. Cutcher-Gershenfeld, E. Greitzer, and J. Kerrebrock, Dec. 2004, *Report to the United States Congress: Aviation and the Environment, A National Vision, Framework for Goals and Recommended Actions*. Partnership for Air Transportation Noise and Emissions Reduction, MIT, Cambridge, MA.
- [5] TRASAS/3 WP08-IATA Work Paper, "Pacific Project," 10th Meeting of the Cross Polar Trans-East ATM Providers' Working Group, Paris, France, November 2010.
- [6] Grabbe, S., B. Sridhar, N. Cheng, August 2006, "Central East Pacific Flight Routing," AIAA-2006-6773, Keystone, Colorado, *AIAA Guidance, Navigation, and Control Conference*.
- [7] Klima, K., 2005, "Assessment of a Global Contrail Modeling Method and Operational Strategies for Contrail Mitigation," M.S. Thesis, MIT.
- [8] Sridhar, B., N. Y. Chen, and H. K. Ng, October 2010, "Fuel Efficient Strategies for Reducing Contrail Formations in United State National Air Space," *29th Digital Avionics Systems Conference*, Salt Lake City, UT.
- [9] Mannstein, H., P., Spichtinger, and K., Gierens K., 2005, "A Note on How to Avoid Contrail Cirrus," *Transportation Research Part D*, Vol. 10, No. 5, pp. 421-426.
- [10] Campbell, S.E., N. A. Neogi, and M. B. Bragg, 2008, "An Optimal Strategy for Persistent Contrail Avoidance," AIAA 2008-6515, *AIAA Guidance, Navigation, and Control Conference*, Honolulu, Hawaii.
- [11] Sridhar, B., H. K. Ng, N. Y. Chen, September 2010, "Aircraft Trajectory Optimization and Contrail Avoidance in the Presence of Winds," *AIAA Aviation Technology, Integration, and Operation Conference*, Fort Worth, TX.
- [12] Sridhar, B., N. Y. Chen, H. K. Ng, A. Morando, "Modeling and Simulation of the Impact of Air Traffic Operations on the Environment," to be published on AIAA Modeling and Simulation Technologies Conference.
- [13] Bryson, A. E., and Y. C. Ho, 1975, *Applied Optimal Control*, Taylor and Francis, Levittown, PA, Ch. 2, pp. 42-89.
- [14] Burrows, J. W., Jan.-Feb. 1983, "Fuel-Optimal Aircraft Trajectories with Fixed Arrival Times," *AIAA Journal of Guidance, Control, and Dynamics*, Vol. 6, pp. 14-19.
- [15] "User Manual for the Base of Aircraft Data (BADA), Revision 3.6," Eurocontrol Experimental Center (EEC) Note No. 10/04, Project ACE-C-E2, Sept. 2004.
- [16] Federal Aviation Administration, Washington, DC, *SAGE System for assessing Aviation's Global Emissions Technical Manual*, 1st ed., September 2005.
- [17] Hadaller, O. J. and A. M. Momenty, 1989, "The Characteristics of Future Fuels," Project Report D6-54940, Boeing publication.
- [18] Baughcum, S., T. Tritz, S. Henderson, and D. Pickett, April 1996, "Scheduled Civil Aircraft Emission Inventories for 1992: Database Development and Analysis," Project Report NASA CR 4700.
- [19] Svensson F., A. Hasselort, and J. Moldanova, 2004, "Reduced Environmental Impact by Lowered Cruise Altitude for Liquid Hydrogen-Fuelled Aircraft," *Aerospace Science and Technology*, 8, pp. 307-320.
- [20] Schumann, U., Feb. 1996, "On Conditions for Contrail Formation from Aircraft Exhausts," *Meteorologische Zeitschrift*, N. F. 5, pp. 4-23.
- [21] Appleman, H., 1953, "The Formation of Exhaust Condensation Trails by Jet Aircraft," *Bull. Amer. Meteor. Soc.*, Vol. 34, 14-20.
- [22] Ponater, M., S. Marquart, and R. Sausen, 2002 "Contrails in a Comprehensive Global Climate Model: Parameterization and Radiative Forcing Results," *Journal of Geophysical Research*, Vol.107, Issue D13, pp. ACL 2-1.
- [23] Duda, D.P., P. Minnis, P. K. Costulis, and R. Palikonda, June-July, 2003, "CONUS Contrail Frequency Estimated from RUC and Flight Track

Data," *European Conference on Aviation, Atmosphere, and Climate*, Friedrichschafen at Lake Constance, Germany.

[24] Degrand, J. Q., A. M. Carleton, D. J. Travis, and P. J. Lamb, "A Satellite-Based Climate Description of Jet Aircraft Contrail and Associations with Atmospheric Conditions, 1977-79," *Journal of Applied Meteorology*, Vol. 39, pp. 1434-1459.

[25] Palikonda, R., P. Minnis, D. P. Duda, and H. Mannstein, August 2005, "Contrail Coverage Derived from 2001 AVHRR Data Over the Continental United States of America and Surrounding Areas," *Meteorologische Zeitschrift*, Vol. 14, No. 4, 525-536.

[26] Alduchov, O. A., and R.E. Eskridge, "Improved Magnus form Approximation of Saturation Vapor Pressure," *Journal of Applied Meteorology*, Vol. 35, 601-609.

[27] Vasatka J., "Polar Operations," Extended Operation Conference, Boeing.

Acknowledgement

The authors would like to acknowledge Mr. Rogier Giepmans for his contribution to the derivation of dynamical equation for optimal aircraft heading.

30th Digital Avionics Systems Conference

October 16-20, 2011